Mouse Slc9a8 mutants exhibit retinal defects due to retinal pigmented epithelium dysfunction

Title:

Mouse *Slc9a8* mutants exhibit retinal defects due to retinal pigmented epithelium dysfunction

Authors:

Shalini Jadeja[1], Alun Barnard[2], Lisa McKie[1], Sally H. Cross[1], Sanger Mouse Genetics Project[3], Morag Robertson[1], Peter Budd[1], Robert E. Maclaren[2], Ian J. Jackson[1,4]*

Affiliations:

[1]MRC Human Genetics Unit, MRC Institute of Genetics & Molecular Medicine, University of Edinburgh, Edinburgh, UK
[2]Nuffield Laboratory of Ophthalmology, University of Oxford, The John Radcliffe Hospital, Oxford, UK
[3] Mouse Genetics Project, Wellcome Trust Sanger Institute, Wellcome Trust Genome Campus, Hinxton, Cambridge, UK
[4]Roslin Institute, University of Edinburgh

* Corresponding Author

Telephone: +44 (0)131 467 8409
Email: ian.jackson@igmm.ed.ac.uk

Word Count: 5764

Abstract

Purpose: As part of a large scale systematic screen to determine the effects of gene knockout mutations in mice, a retinal phenotype was found in mice lacking the *Slc9a8* gene, encoding the sodium/hydrogen ion exchange protein NHE8. We aimed to characterise the mutant phenotype and the role of sodium/hydrogen ion exchange in retinal function.

Methods: Detailed histology characterised the pathological consequences of *Slc9a8* mutation, and retinal function was assessed by electroretinography (ERG). A conditional allele was used to identify the cells in which NHE8 function is critical for retinal function, and mutant cells analysed for the effect of the mutation on endosomes.

Results: Histology of mutant retinas reveals a separation of photoreceptors from the retinal pigment epithelium (RPE) and infiltration by macrophages. There is a small reduction in photoreceptor length and a mislocalisation of visual pigments. ERG testing reveals a deficit in both rod and cone pathway function. The RPE shows abnormal morphology, and mutation of *Slc9a8* in only RPE cells recapitulates the mutant phenotype. NHE8 localises to endosomes, and mutant cells have much smaller recycling endosomes.

Conclusions: NHE8 is required in the RPE to maintain correct regulation of endosomal volume and/or pH which is essential for the cellular integrity and subsequent function of RPE.

Introduction

In an international effort to assign function to all genes, and to identify new models of human disease, cohorts of mice produced from mutant embryonic stem cells are being screened in large-scale phenotyping pipelines. Hundreds of mouse lines, each mutant for a different gene, have been analysed for developmental, haematological, immunological, metabolic, neurological, reproductive and sensory parameters which thus provide a comprehensive assessment of the consequences of gene ablation [1]. Included in the sensory analysis is slit lamp examination of the anterior chamber of the eye and indirect ophthalmoscopy to view the retina and retinal vessels. The phenotype data can be viewed online and the mice are freely available. We describe here the detailed pathological and functional analysis of a mouse line mutant in the sodium/hydrogen ion exchange protein gene, *Slc9a8*, which was identified as having a retinal defect and no other abnormality other than male sterility.

Sodium/hydrogen ion exchange proteins (NHEs) or cotransporter solute channels are encoded by the *Slc9* gene family, comprising nine members: *Slc9a1-9*, encoding NHE1-9. NHE1 to 5 are located in the plasma membrane whilst NHE6 to 9 are found in membranes of cell organelles (reviewed in [2]). These proteins contain 12 membrane spanning domains and catalyse the electroneutral transport of cations down a concentration gradient. Typically sodium ions are transported in and hydrogen ions out of the cell or organelle. Simultaneous transport of anions creates osmotic pressure and results in influx of water, regulating the pH and volume of cells and organelles.

Sodium/hydrogen ion exchange is involved in aqueous humour dynamics and maintenance of intraocular pressure (IOP). Inhibition of sodium/hydrogen ion exchange in mice[3] reduces IOP and at least one cotransporter, NHE1, is found expressed in the ciliary body, where aqueous dynamics are regulated. The single yeast NHE is necessary for correct sorting of proteins to the vacuole[4] and indeed depletion of NHE8 in mammalian cells disrupts endosome trafficking[5]. Six of the *Slc9* family members have been mutated in mice and give rise to a range of phenotypes, from hyperactivity or ataxia and seizures (*Slc9a1 and 6*) [6,7,8] to relatively mild gastric secretion and absorption defects (*Slc9a2*, *3* and *4*) [9,10,11].

Slc9a8 is widely expressed in adult mouse tissues but is enriched in kidney, intestine, muscle, liver and testes[12, 13]. The gene is expressed in the kidney proximal tubules, where reabsorption of secreted bicarbonate requires NHE function, although this is mostly via Slc9a3 (NHE3). *Slc9a8*, is, however, expressed at higher levels in the neonatal kidney, and may partially compensate for NHE3 in *Slc9a3* knockout animals which have only a mild absorption defect[14]. The *Slc9a8* gene has previously been knocked out and the authors report that the mice have normal levels of serum sodium ions. They also report an increase in the length of the intestine, but a reduction in the number of goblet cells in the mutant mice with a concomitant reduction in mucin secretion and pH[13, 15]. Furthermore it has recently been reported that the gene is expressed in the epithelial cells of the conjunctiva, cornea and lacrimal glands and may play a role in the protection of these ocular epithelia[16] The male mutants are also sterile.

Here we identify and characterise a previously undescribed retinal defect of *Slc9a8* knockout mice and locate the origin of the phenotype to be abnormalities in the retinal pigmented epithelium.

Materials and Methods

Animals

Slc9a8$^{tm1a(KOMP)Wtsi}$ mutant mice were obtained from the Wellcome Trust Sanger Institute which were generated as part of the Eumodic phenotyping screen. We maintained the mice on a C57BL6/J background. Germline Cre expressing mice were made by DJ Kleinjan, MRC Human Genetics Unit[17], tyrosinase Cre expressing mice were from L. Larue, Institut Pasteur[18] and R26MTMG reporter mice originally from L. Luo, Stanford University[19]. The FLPe expressing mice were made by A. Smith, University of Edinburgh[20]. All experiments complied with the ARVO Statement for the Use of Animals in Ophthalmic and Vision Research and the relevant local animal welfare conditions. Mice were genotyped by PCR using the primers in Supplementary Table S1.

RNA Expression

RNA was prepared from adult eyes using the RNeasy Plus Mini kit (Qiagen) following the manufacturer's instructions. First strand cDNA was prepared from 300 ng RNA using the First Strand cDNA Synthesis Kit for RT-PCR (AMV) (Roche) following the manufacturer's instructions. 5% of this was used as a template for PCR using DreamTaq Green DNA Polymerase (ThermoScientific) with primers at 200 nM. The PCR amplification conditions used were as follows. One cycle of 94°C for 4' followed by 30 cycles of 94°C 30'', 58°C 30'', 72°C 30" followed by one cycle of 72°C 10'. PCR

products were analysed on 2% agarose gels. Primers used are in Supplementary Table S2

Electroretinography

Before testing, mice were dark adapted overnight (>18 hr) and anaesthetised via intraperitoneal injection (80 mg/kg ketamine and 10 mg/kg xylazine). Pupils were dilated with 1% tropicamide and 2.5% phenylephrine eye drops. A DTL-type silver-coated nylon thread active electrode was modified to include a custom-made contact lens of clear Aclar film. This was positioned concentrically on the cornea using hypromellose eye drops (1% methylcellulose solution) for coupling. Platinum needles in the scruff and at the base of the tail served as reference and ground electrodes, respectively. Animals were maintained at 37°C using a heated blanket with feedback rectal probe. Signals were differentially amplified and digitized at a rate of 5 kHz using an Espion E2 console (Diagnosys LLC, Cambridge, UK) that controlled the timing of the light stimulus generated by a Grass PS33 photic stimulator dome. The intensity of the unattenuated, brief (10 μs), bright, white single-flash was 1.03 log lumen s/m^2. This was attenuated using neutral density filters to generate the dim flash (-2.57 log lumen s/m^2). Inter stimulus intervals were 6s and 60s for dim and bright flashes, respectively. Averaging of 16 and 4 flashes was used for dim and bright stimuli, respectively. For light-adapted recordings, animals were exposed to a steady white background (~150 lux) for 10 min after which flashes of the bright stimulus were superimposed at a rate of 1 Hz with 20 flashes averaged per response.

Confocal scanning laser ophthalmoscope imaging

Imaging was performed using a Spectralis HRA confocal scanning laser ophthalmoscope (Heidelberg Engineering, Heidelberg, Germany). Mice were anaesthetised and eyes dilated as above. A custom made PMMA contact lens was placed on the cornea with 0.3% methylcellulose gel as viscous coupling fluid. The mouse was positioned on a platform mounted on the chin rest of the cSLO device. All images were recorded using the 55° lens. The NIR reflectance image (820 nm diode laser) was used to align the fundus camera relative to the pupil and to focus on the confocal plane of interest. Fluorescence was excited using a 488 nm argon laser or a 790 nm diode laser and emission was recorded at 500 to 700 or greater than 810 nm, respectively. Images were recorded using “automatic real time” (ART) mode, which tracks ocular movement (e.g., due to respiration) and averages consecutive images resulting in an improved signal-to-noise ratio.

Colour fundus imaging

Images of the fundus were collected by using a topical endoscope (BERCI Tele-Otoscope with HOPKINS straight forward 0°, diameter 3mm, Halogen cold light fountain light source) and camera (Nikon D40x with Nikon AF 85mm F1.8D AF Nikkor lens)

Tissue preparation and staining

Mice were sacrificed at the appropriate age and the eyes were enucleated and fixed in Davidson’s fixative (28.5% Ethanol, 2.2% Neutral buffered formalin, 11% Glacial acetic acid) overnight at 4°C. The eyes were then dehydrated through an ethanol series and embedded in paraffin for 7µm sectioning on a Leica RM 2235 microtome

for histological analysis. Haematoxylin and Eosin staining were performed according to standard procedures.

Immunofluorescence

Citrate buffer antigen retrieval was used for paraffin sections. We blocked all the sections in 10% heat inactivated donkey serum in phosphate buffered saline (PBS) plus 3% Triton X-100 for an hour, and performed all antibody incubations in the same solution at room temperature for an hour in block or overnight at 4 °C.

Wholemount RPE was dissected from unfixed eyes and then fixed in cold (-20 °C) methanol for at least 30 minutes prior to immunofluorescence staining. Wholemount buffer (3% Triton-X100, 0.5% Tween-20, 1% Bovine Serum Albumin in PBS) was used to block, wash and for all antibody incubations. Briefly, RPE was rehydrated in PBS, blocked for an hour and primary antibodies incubated at room temperature overnight. Following washes, secondary antibodies were incubated for 2 hours, washed in wholemount buffer twice and PBS twice before being mounted and imaged.

Tissue from at least five mice of each genotype from at least three different litters was used for all analysis. All tissues were mounted in Vectashield (Vector Laboratories, UK), imaged by confocal microscopy (Nikon A1R) and maximum intensity projections of z-stacks were created using NisElements AR Version 4.0 software. All images are representative of at least three animals.

For immunoflourescence the following antibodies were used; Rabbit anti-Slc9a8 (AbD Serotec, UK, 1:200), Mouse anti-Rhodopsin (Millipore, UK, 1:500), Rat anti-F4/80 (AbD Serotec, UK, 1:500), Rabbit anti-ML- Opsin (Millipore, UK, 1:500), Goat anti-S-Opsin (Insight Biotechnology, UK, 1:500), Mouse anti-Beta-catenin (Sigma, UK, 1:200), Rabbit-anti-ZO-1 (Invitrogen, UK, 1:100), Rat anti-Transferrin receptor (Lifespan Biosciences, UK, 1:200) and Mouse anti-Golgin 97 (Invitrogen, UK, 1:200). Alexa fluor secondary antibodies (Invitrogen, UK, 1:500) were used.

Retinal Thickness Measurement

Sections from 25 week old mice were stained with Haematoxylin and Eosin and two images were taken from each eye near the centre of the retina, adjacent to the optic nerve head, and two from the retinal periphery. For each image 5 measurements of each retinal cell layer was taken using ImageJ[21] A minimum of 5 eyes of each genotype were measured and the mean of these measurements was used.

Intra-ocular Pressure Measurement

Intra ocular pressure (IOP) measurements were obtained as previously described[22], with modifications. The mice were anesthetised by intraperitoneal (IP) injection of a 0.1ml/ 10 gram bodyweight of a 100 mg/ml ketamine/ 10mg/ml xylazine mixture. The rebound tonometer, TonoLab (Icare, Finland), was used to take a set of 6 measurements of IOP in each eye. IOP measurements were always taken at the same time of day, between 13.00 and 15.00. All cohorts included male and female mice. 1-3 months wt: 30, hom 36 eyes measured, 3-6 months: 28 eyes of each genotype measured.

Plasmid construction

An NHE8-haemaglutinin construct was obtained[5] and the human *Slc9a8* coding region lacking the translation stop codon was cloned as a PCR fragment into XhoI-BamHI sites into the vector pmKATE2-N (Evrogen, UK). The GalT-GFP TGN expression marker was obtained from Mark Handley (MRC HGU Edinburgh).

Cell culture

Human RPE1 cells were grown in DMEM:F12 (Invitrogen, UK) supplemented with 10% fetal calf serum (FCS) and 1% penicillin/ streptomycin in a humidified 5% CO_2 incubator at 37°C. Mouse embryonic fibroblasts (MEFs) were isolated from E13.5 embryos. Embryo heads and organs were removed prior to trypsin digestion at room temperature for 30 minutes. Digested samples were plated in Optimem (Invitrogen, UK) supplemented with 10% FCS, 1% penicillin/ streptomycin and 0.00074% beta-mercaptoethanol in a humidified 5% CO_2, 3% O_2 incubator at 37°C. RPE1 cells were transfected using Lipofectamine 2000 (Invitrogen, UK) following the manufacturer's instructions. Cells were imaged live 48 hours after transfection in HBSS containing calcium and magnesium ions.

Organelle volume and intensity measurements

5 MEF lines of each genotype from 3 litters were used at passage 3-5 and were plated at a density of 2 x 10^4 cells/ well of a 24-well plate. 48 hours following plating, FITC conjugated rat anti-Transferrin receptor antibody was added to the growth medium at a dilution of 1:200 and incubated at room temperature for 30 minutes. The cells were washed and incubated in HBSS containing calcium and magnesium ions for imaging. For each MEF cell line a minimum of 10 independent images were

taken. The Volocity 3D Image analysis software (PerkinElmer) was used to quantify the number, volume and mean FITC-intensity of each recycling endosome.

Results

Slc9a8 mutant mice exhibit an eye phenotype

An international effort to produce "knockout" mutations of all the genes in the mouse genome has generated libraries of embryonic stem cells and mice containing targeted mutations. In many cases the vectors are designed to eliminate gene function ("knockout first") but with the capability of engineering the allele in mice to produce a Cre-recombinase conditional allele, so that temporally or spatially restricted knockouts can be generated, and a more robust knockout mutation can be made by deleting a critical exon[23]. Mice carrying the "knockout first" mutant allele of *Slc9a8* (*Slc9a8*$^{tm1a(KOMP)Wtsi}$) were generated. In this allele exon 3 of *Slc9a8* splices onto *LacZ* in the targeting construct to generate a reporter-tagged mutation. We subsequently generated mice carrying the *Slc9a8*$^{tm1d(KOMP)Wtsi}$ allele, by sequential crossing with animals expressing the recombinases Flp and Cre in the germ line. In this allele the targeting cassette and the 59bp exon 4 are deleted, resulting in a frame-shift. Reverse-transcription polymerase chain reaction (RT-PCR) amplification of mRNA from wild-type, heterozygous and homozygous mutant eyes shows that no *Slc9a8* mRNA is made in knockout first (tm1a) eyes (Figure 1A). RNA from eyes of exon 4 deleted (tm1d) mice produced amplification products smaller by 59bp, indicating transcription of the internally deleted, frameshift, mRNA (Figure 1A). Mice homozygous for the knockout first allele were tested in the Wellcome Trust Sanger Institute (WTSI) pipeline of phenotype assessments[1]. This battery of tests

provides a first-pass analysis of a wide range of phenotypic parameters. *Slc9a8* mutant mice are morphologically normal, and show no phenotypic deviation from wild type in all but two tests (http://www.mousephenotype.org/data/genes/MGI:1924281). Firstly, male mutant mice are almost completely infertile. From 25 matings between mutant males and females of either heterozygous or homozygous genotypes, 24 gave no offspring and one mating between a homozygous male and a heterozygous female produced a single litter with two pups. By contrast, 8 homozygous females mated with wild type males produced 13 litters with a total of 87pups (6.7 per litter), and a further 38 homozygous females mated with heterozygous males produced 445 pups in 65 litters (6.8 per litter). Three of these 46 females produced no offspring.

Secondly, all mutant mice examined by indirect ophthalmoscopy (7 male and 7 female) showed abnormal pigmentation of the retina (Figure 2 A, B). All homozygotes had many darkly pigmented patches throughout the retina, possibly indicative of retinal degeneration or abnormalities of the retinal pigmented epithelium (RPE). Mutant mice generated for this screen are produced on a genetic background which is a mixture of C57BL6/J and C57BL6/N strains. The latter contains the *rd8* deletion mutation in the *Crb1* gene and which results in late onset retinal degeneration and abnormal retinal lamination[24,25]. Although *Crb1*^{rd8} mutants clearly differ from the *Slc9a8* mutant in retinal phenotype and age of onset it was important that this mutation be removed to avoid confounding the analysis. We thus backcrossed the original strain onto C57BL6/J and identified mice which were wild-type at *Crb1* but carried the *Slc9a8* mutation. Subsequent analyses were on mice without the *Crb1*^{rd8} mutation and on a C57BL6/J background.

Slc9a8 is widely expressed throughout many tissues. We examined the sites of expression of the gene in the eye by staining heterozygous knockout first eyes for expression of the beta-galactosidase gene inserted into the locus. Figure 1B clearly shows blue staining of expression in the photoreceptors and the ganglion cells of the retina. Unfortunately the melanin of the retinal pigmented epithelium (RPE) (absent from Figure 1B) obscures staining for expression in those cells.

To further analyse the retinal phenotype we examined mutant eyes by scanning laser ophthalmoscopy (SLO). Infra-red (IR) reflectance imaging showed grainy and highly reflective dots in mutant retinas, which were not present in control mice (Fig. 2C, D). Autofluorescence (AF) imaging with a 488 nm laser revealed marked abnormalities in the mutant retina; uniform background AF appeared to be reduced compared to WT controls but many small hyperautofluorescent puncta were present across the retina (Fig. 2E, F), perhaps suggesting the infiltration of autofluorescent macrophages into the retina and/or the activation of resident microglia. AF imaging with the near infra-red 790 nm laser again showed hyperautofluorescent puncta spread throughout the retina of mutant mice and also more extensive regions of hyperautofluorescence (Fig. 2G, H). High 790 nm AF is likely indicative of RPE pathology in mutant mice. Puncta and patches of high 790 nm and 488 nm AF resided in the outermost retina/RPE and often, but not always, co-localised.

Retinal Histology of *Slc9a8* Mutant Mice

We investigated the retinal pathology in more detail by examining histological sections. The most striking histopathological change was in the RPE. Whilst wild-type

sections show close apposition between the RPE and the neural retina, mutant retinas have a distinct separation of these cell layers. Some areas have wide detachment, which may be an artefact of sample preparation, but elsewhere, throughout the retina, there is a clear gap between the photoreceptors and the RPE (Figure 3A-D). Within this space and penetrating far into the photoreceptor layer are many pigmented cells (white arrows, Figure 3B,D). We investigated the identity of these cells by staining retinal sections of mutant mice with an antibody against the macrophage membrane protein F4/80, and counterstained for rhodopsin (Figure 3E). Positive staining for F4/80 in the ectopic pigmented cells suggests they are macrophages, consistent with the observations by SLO. They are likely to have become pigmented by engulfing melanin or melanin containing cells. Immunostaining shows they also contain rhodopsin, suggesting that they have engulfed photoreceptor outer segments (Figure 3E).

The mutant retinas show some loss of photoreceptors, as indicated by a slight thinning of the outer nuclear layer (ONL). This was most pronounced in older mice (over 25 weeks of age), but even in these mice the reduction in ONL was no more than 16% (Supplementary Table S3, schematically shown in Figure 3F). The photoreceptor outer segment layer was also thinner, indicating that although there has been some loss of these cells, there is also an overall shortening of the photoreceptors (Figure 3G).

To investigate the effect of the mutation on both rods and cones, we stained retinal sections with antibodies against rhodopsin and cone opsins (Figure 4A-D). Both rods and cones are affected in the mutant mice. The photoreceptor outer segments are

shorter than normal and there appears to be a reduction in the number of cones, stained for cone opsins (Figure 4A,B). In addition there is a striking mislocalisation of opsins within the cones (Figure 4C,D).

RPE Morphology is Abnormal in *Slc9a8* Mutant Mice

To examine the RPE in more detail we prepared flat-mounts of this tissue and stained for ZO1, to examine the tight junctions between cells in this epithelium. In wild-type RPE the cell junction staining reveals the typical hexagonal morphology of the RPE (Figure 4E). DAPI staining for DNA shows some cells are binuclear, or two cells are within a single, hexagon of ZO1 deposition, but all lie within a regular and contiguous pattern. By contrast, in mutant RPE there are regions where numerous nuclei are seen enclosed within a large segment of ZO1, suggesting larger multinucleated cells (Figure 4F). This suggests a loss of RPE cells as RPE cell death is often accompanied by the increase in size of the neighbouring cells in order to prevent gaps appearing in the epithelium[26].

Impaired Retinal Function in *Slc9a8* Mutant Mice

To examine retinal function we carried out electroretinography (ERG) in mutant (N=7) and control (N=8) mice at 23-25 weeks of age. Dark-adapted ERG responses were recorded to dim and bright flash stimuli; intensity-dependent responses could be seen in mutant mice but there were clear deficits in the size and speed of responses when compared to wildtype animals (Figure 5, data in Supplementary Table S4).

In dark-adapted conditions, the initial negative deflection of the ERG (the a-wave) is indicative of rod photoreceptor function. In mutant mice, the amplitude of the a-wave was significantly reduced in response to both dim (Figure 5A,B) and bright stimuli (Figure 5D,E). The time until the peak of the a-wave (implicit time) was significantly increased in mutant mice in response to the bright stimulus (Figure 5E) although the timing of responses to dim stimuli was not significantly different (Figure 5B).

Following the negative a-wave is a strong positive deflection known as the b-wave. The positive peak of the b-wave primarily reflects the activation of bipolar cells (second-order neurones that are immediately downstream of photoreceptors), particularly ON-type, depolarising bipolar cells. By convention the magnitude of the b-wave is measured from the trough of the preceding a-wave, where present. For this reason, a deficit in the a-wave will almost inevitably lead to a respective abnormality in the b-wave. Consequently, we observed a significantly smaller b-wave in mutant mice in both dim (Figure 5C) and in bright flash conditions (Figure 5F). Mutant mice also had slower b-waves; the implicit time of the b-wave was significantly increased in response to both dim and bright stimuli (Figure 5C,F).

Deficits in the size and speed of the b-wave might point to a defect in bipolar cell signalling and/or function. However, in order to distinguish between a disorder that is localised primarily to the photoreceptors and one that also impacts on more proximal retinal cells it is important to consider the proportionality between a- and b-waves. We therefore calculated the size of the dark-adapted, bright flash ERG b-wave as a ratio of the a-wave amplitude recorded in the same individual (b/a-wave ratio). This

revealed that in wild types the ratio was 1.93 ± 0.04 (mean±SEM, n=8) and was increased by >50%, to 3.07 ± 0.11 (mean±SEM, n=7) in mutant mice (Figure 5I). This highly significant increase (p=0.0001, unpaired t test with Welch's correction) suggests that bipolar cells are not directly affected by the mutation and there may even be some compensatory increase in the amplification of signal transmission in the outer plexiform layer.

To isolate retinal responses of the cone pathway, after dark-adapted recordings were finished, mice were exposed to a rod-saturating background illumination for at least 10 min and ERGs were then recorded for bright flash stimuli superimposed on the background. In these light-adapted conditions, the ERG response in mice is dominated by the positive b-wave and little or no negative a-wave is observed (Figure 5G). Therefore, activity of cone photoreceptors cannot be directly recorded but activation of ON bipolar cells of the cone pathway can be measured by the b-wave. In light-adapted ERG recordings, the responses of mutant mice were again both significantly smaller and slower than wild type controls. The amplitude of the b-wave was reduced by around 42% and the b-wave implicit time was increased by ~24% (Figure 5H).

Overall, we found highly significant differences between mutant and wild-type animals, in terms of both rod and cone pathway function (P-values in Supplementary Table S4). In all tests, mutant ERG responses were smaller and slower than those of wild type control animals. In particular, the ratio of b/a-wave amplitudes in dark-adapted ERGs points to a deficit in photoreceptor cells in mutant mice. When we examined histologically the eyes of mice which had undergone ERG testing, we

found that, as before, photoreceptor cell number (as measured by outer nuclear layer thickness) is only mildly reduced in mutant mice (data not shown). In general, the deficits in retinal function appear to be much greater than the retinal degeneration observed on histology (for example there is a ~68% reduction in the dark-adapted ERG but only a <16% reduction in the ONL thickness). This indicates that the major cause of ERG abnormalities is not photoreceptor cell loss, but rather a substantial deficit in individual photoreceptor function. This is combined with a mild degree of photoreceptor cell loss, which could be caused as a primary result of the mutation or as a secondary consequence of impaired RPE function.

Slc9a8 Mutant Mice have Normal Intraocular Pressure

Sodium hydrogen ion exchange is required to maintain the IOP, and inhibition of NHE function causes reduction in IOP. We considered the possibility that the retinal defect observed in *Sc9a8* mutant mice was secondary to a reduced IOP. We measured the IOP of mutant and control animals by tonometry and found that there was no difference in pressure between the two groups of mice (Supplementary Figure).

RPE Specific Knockout of Slc9a8 Results in Retinal Defects

To investigate the primary cause of the retinal pathology in *Slc9a8* mutant mice, we generated mice in which the gene was deleted only in the RPE, and not in the neural retina. This we achieved by initially converting the knockout first allele to a conditional allele (*Slc9a8*$^{tm1c(KOMP)Wtsi}$) by crossing with mice expressing a germ-line FLP-

recombinase. This recombinase deletes the DNA between the *frt* sites which flank the beta-geo selection cassette in the targeted allele to produce a gene with restored function, containing only *loxP* sites flanking exon 4. We confirmed that this allele functioned normally by examining the eyes of homozygous conditional mice in absence of Cre-recombinase, which we found to be unaffected (Figure 6A, C). We then crossed these animals with mice carrying the *Tyr-Cre* transgene, which expresses Cre recombinase from the tyrosinase promoter, active in melanocytes and RPE cells. To confirm the tissue specificity of the *Tyr-Cre* we crossed it to mice with the R26MTMG transgene. This transgene expresses the fluorescent tomato protein in all cells, from the Rosa26 promoter, except in the presence of Cre recombinase when the tomato is deleted and the cells express green fluorescent protein instead[19]. Examination of the retinas of mice with the *Tyr-Cre* and R26MTMG transgene indicated that the Cre recombinase was only active in the RPE (which was green) and not in the neural retina (all layers of which were red) (Figure 6E).

By crossing mice with the conditional allele of *Slc9a8* with *Tyr-Cre* we generated animals which were homozygous for conditional *Slc9a8* and expressed Cre recombinase in the RPE. On examination of these eyes we found a phenotype indistinguishable from that with the constitutive knockout-first allele, by indirect ophthalmoscopy (Figure 6B, compare with Figure 2B) and by histology (Figure 6C, compare with Figure 3B and D). Note in particular the separation of RPE from the photoreceptors, and the presence of pigmented cells, probably macrophages containing engulfed melanin, in the photoreceptor layer, as seen in the global knockout phenotype in Figure 3B and D. We conclude that loss of *Slc9a8* in the RPE

is sufficient to cause the histological retinal phenotype we observe, although we have not analysed ERGs of these animals.

Loss of *Slc9a8* Results in Changes in Recycling Endosomes

One major function of the RPE in retinal physiology is in the visual cycle, whereby there is a transfer of retinals between photoreceptors and RPE with isomerisation and re-isomerisation between 11-*cis* and all-*trans* retinal. A second important function is the phagocytosis of outer segment discs shed by the photoreceptors. Both these functions require recycling endosomes in the RPE. Others have previously reported that the *Slc9a8* encoded protein (NHE8) localises to the trans-Golgi network (TGN) and to late endosomes in HeLa cells, and that treatment of these cells with siRNA against *Slc9a8* results in an endosomal phenotype[5]. We confirmed this localisation in RPE1 cells; NHE8 tagged with either HA for immune-detection, or with mKate for direct fluorescent imaging was found in the TGN (Figure 7A-E). In agreement with others we also found NHE8 in late, (recycling) endosomes, colocalised with transferrin receptor, in RPE1 cells (Figure 7F-H).

To observe the effect of loss of *Slc9a8* on endosomes we isolated mouse embryonic fibroblasts (MEFs) from wild type and mutant embryos, and stained for golgin97 and transferrin receptor. Sodium/hydrogen ion co-transporters regulate both pH and volume of organelles by affecting the distribution of ions. We measured the volume of recycling endosomes, stained with transferrin receptor antibodies, and found them to be reduced in size in mutant cells compared to wild-type. The mean volume per

mutant endosome is approximately 50% that of the controls (Figure 8, one way ANOVA P=0.04).

Discussion

Slc9a8$^{tm1a(KOMP)Wtsi}$ Mutant Mice Exhibit a Prominent Retinal Phenotype.

We have shown here that mice lacking *Slc9a8* manifest a noticeable ocular phenotype, which consists of retinal degeneration and/or detachment, abnormal opsin localisation, subretinal macrophage infiltration and severely reduced retinal electrophysiological activity. The phenotype is associated with abnormal recycling endosomes in the retinal pigment epithelium, and we speculate that this deficit impairs the ability of the RPE to fulfil one or more of its normal support functions (see below). A defect in the ocular surface of *Slc9a8* KO mice has been reported recently which results in decreased tear production and potential defects in ocular epithelial protection[16] but we did not observe any morphological abnormalities of the cornea. The only other abnormal phenotype detected by the high-throughput screening carried out at the Wellcome Trust Sanger Institute (WTSI) is male infertility. The fertility defect has recently been examined in detail and appears to be associated with defects in luteinising hormone receptor and a concomitant reduction in testosterone[27].

Others have found that a gene-trap mutation of *Slc9a8* had defects in the gastrointestinal tract, including a reduction in the number of goblet cells, reduction in mucin production and decreased surface pH along with an ~18% increase in length of the small intestine and a doubling in the weight of the caecum[13]. The reduction in mucin appeared to lead to an increase in bacteria attached to the distal colon and a sensitivity to dextran sulphate[28]. The mutant mice also had a higher incidence of gastric ulcers than controls[15]. None of these phenotypes were observed in the mice screened at WTSI, although the high-throughput nature of the screen meant that these parameters were not measured. Nevertheless, the mice had normal weight and growth. Furthermore, the mutant strain was subjected to bacterial challenge; by intravenous infection with *Salmonella* and oral infection with *Citrobacter* and showed no difference in infection. In particular following *Citrobacter* infection the colon and caecum were closely examined for bacterial load and for hyperplasia and the mutant mice were no different from controls. It is worth noting that the genetic background of the two studies differ; in the previous studies the mutation was generated on a 129S1 background but maintained on a mixed, outbred, 129/Black Swiss background whilst in the current study the mutation was made and initially screened on a C57BL6/N background and subsequently maintained by backcrossing on to the closely related C57BL6/J strain.

Given the widespread expression of *Slc9a8* it is surprising that we detected no defects in any other systems, in particular in kidney function where the gene is expressed at higher levels and the protein is localised to the apical membrane of the proximal tubule[14,12]. The abundance of other NHE family members may mean that in

most tissues there is sufficient function provided by other cotransporters to compensate for loss of NHE8.

Slc9a8 is not required for maintenance of IOP

Maintenance of intraocular pressure requires sodium/hydrogen ion exchange. Aqueous humor is secreted by the ciliary epithelium and drains out at the iridocorneal angle through the trabecular meshwork into Schlemm's canal. The balance between secretion and drainage is the key factor in regulating the volume, and hence the pressure, of the aqueous humor. Blockage of drainage is a common cause of raised IOP. Secretion of the aqueous humor must be tightly regulated to prevent over or under production with consequential increase or decrease in volume and pressure. Avila et al[3] showed that pharmacological inhibition of the sodium/hydrogen ion exchange protein NHE1 (SLC9A1) reduced IOP. As *Slc9a8* is expressed in the ciliary epithelium, and the activity of the drugs against this target was not characterised, it was reasonable to postulate that this protein might be the key cotransporter in the ciliary body regulating aqueous humor secretion, and that the retinal pathology we observe in the mutants might be a consequence of lowered IOP. However, we found no change in IOP measurements between mutant and control mice, indicating that NHE8 is not the prime regulator of IOP.

An RPE Defect Underlies the Eye Pathology

Cell-type specific knock-out of *Slc9a8* in only the RPE recapitulates the phenotype seen in a global knock-out, indicating that absence of the gene in the RPE is

sufficient to cause the retinal defect. Histology reveals evidence of RPE cell death, shown by large multi-nucleated RPE cells in mutant mice, possibly caused by the compensatory expansion of cells to replace dying neighbour cells. Others have shown that NHE8 localises to both the trans Golgi network and to the endosomal compartment in HeLa cells[5] and we confirm this in RPE1 cells. Knockdown of NHE8 using siRNA in HeLa cells results in perinuclear clustering of recycling endosomes. We do not observe such clustering universally in fibroblasts from *Slc9a8* knockout mice, but we do see a significant decrease in the size of endosomes.

Lawrence et al[5] do not report a pH change, and it is possible that cell types vary in their requirement of NHE8 in endosomes. Certainly an endosomal defect may underlie the mutant phenotype we observe. Phagocytosis and recycling of photoreceptor outer segments is one of the key functions of the RPE and even a small deficiency in this function could result in abnormal photoreceptor function. This has been demonstrated in other mouse models of retinal degeneration, including the mouse myosin VIIa (*Myo7a*) mutant which models Usher syndrome. The RPE of *Myo7a* null mice is unable to phagocytose photoreceptor outer segments efficiently and is thought to contribute to progressive blindness[29]. NHE8 is not the first ion channel implicated in retinal degeneration. Bestrophin forms an oligomeric chloride channel on the basolateral membrane of the RPE cells and mutations in this gene cause various types of macular degeneration[30,31,32]. In particular, BEST1 mutant proteins exhibit chloride channel defects which underlie their degeneration phenotypes[33]. It is clear therefore that ion exchange in the RPE is important for RPE function, and disturbance in the process can result in disease.

Targeted knockout of another solute carrier gene, *Slc4a5*, shows a similar eye pathology to the one we describe here[34]. *Slc4a5* encodes an electrogenic sodium bicarbonate cotransporter that is necessary for normal function of the choroid plexus and maintenance of cerebrospinal fluid composition and intracranial pressure. The eyes of these mutant mice have retinal detachment and a functional ERG deficit, similar to our Slc9a8 mutant, but the critical cells though which the phenotype is mediated have not been identified.

Acknowledgements

We would like to thank Craig Nicol for help with photography and illustrations, Iain McCall for animal husbandry, Simon John and Mimi de Vries for tonometry advice, Katherine Bowers (UCL, London) for the NHE8-HA construct and Mark Handley (MRC Human Genetics Unit) for the GalT-GFP. We also thank the Wellcome Trust Sanger Institute's Research Support Facility and Mouse Informatics Group for their excellent technical support.

1

Figure Legends

Figure 1 Expression of Slc9a8 in knock and wild-type eyes

RT-PCR from adult eye samples (**A)** showing that *Slc9a8* is knocked out in the *Slc9a8*$^{tm1a(KOMP)Wtsi}$ and *Slc9a8*$^{tm1d(KOMP)Wtsi}$ alleles. Shown are RT-PCR products produced using primer pairs from exon 2 and 6, exon 3 and 6, exon 5 and 6 of *Slc9a8* and exon 7 and 9 from *Hprt* as a control. Primer sequences are in Supplementary Table 2. Genotypes of samples are as follows; wild-type (WT), heterozygous *Slc9a8*$^{tm1a(KOMP)Wtsi}$ (1a/+), homozygous *Slc9a8*$^{tm1a(KOMP)Wtsi}$ (1a/1a), heterozygous *Slc9a8*$^{tm1d(KOMP)Wtsi}$ (1d/+), homozygous *Slc9a8*$^{tm1d(KOMP)Wtsi}$ (1d/1d), no template (-). (**B**) Section of retina from heterozygous *Slc9a8*$^{tm1a(KOMP)Wtsi}$ mice, stained for beta-galactosidase. Blue stain reveals expression in the photoreceptors (PRL) and retinal ganglion cells (GCL). Scale bar 50μm.

Figure 2: Retinal defects in *Slc9a8*$^{tm1a(KOMP)Wtsi}$ mice

Fundus image of a control retina (**A**) showing normal retinal morphology. Initial phenotyping by the Sanger Mouse Genetics Project identified retinal defects in *Slc9a8*$^{tm1a(KOMP)Wtsi}$ homozygous mutant mice, as evidenced by the presence of dark patches (arrowheads)(**B**). **C-H**: Scanning laser ophthalmoscope images of wild type control (**C**,**E**,**G**) and *Slc9a8* mutant (**D**,**F**,**H**) eyes. **C** and **D**: infrared reflectance imaging, **E** and **F**: autofluorescence at 488nm, **G** and **H** autofluorescence at 790nm.

Figure 3: Retinal Histology of *Slc9a8*$^{tm1a(KOMP)Wtsi}$ mice

Histological analysis of haematoxylin and eosin stained sections identified the onset of the degeneration at around 8 weeks. Control retinas show normal lamination (**A**) whereas *Slc9a8*$^{-}$ mutant retinas exhibit thinning of the photoreceptor layer (PRL) with

infiltration of the retinal pigment epithelium (RPE) (arrowheads) (**B**). By 1 year of age, control retinas (**C**) still show full thickness of the PRL but mutant retinas (**D**) exhibit further thinning of this layer and continued RPE infiltration. Immunofluorescence shows positive staining for macrophages (F480) (red) containing rhodopsin (green) in the RPE infiltrates suggesting phagocytosis of photoreceptors (**E**). Measurement of retinal cell layers shows a slight decrease in overall retinal thickness in the central and peripheral *Slc9a8* homozygous mutant (Hom) compared to wildtype controls (WT) (**F**). The decrease in the photoreceptor layer in the centre of the retina is statistically significant (One way ANOVA, *p< 0.05)(G) Numerical data are in Supplementary Table S3. Photoreceptor layer (PRL), outer nuclear layer (ONL), outer plexiform layer (OPL), inner nuclear layer (INL), inner plexiform layer (IPL) and ganglion cell layer (GCL). Scale bars: 50 μm.

Figure 4: Characterisation of retinal degeneration in *Slc9a8*$^{tm1a(KOMP)Wtsi}$ mutant mice

Immunofluorescence of a control retinal section shows regular expression of all three opsins (Rhodopsin, blue; ML-opsin, green and S-opsin, red) (**A**). *Slc9a8* mutant retinas shows reduced numbers of opsin positive cells. (**B**). Higher magnification shows the regular cone morphology in ML-opsin positive cells (green) in control retinas (**C**). Cone outer segments appear irregular in *Slc9a8* mutant mice with accumulation of ML-opsin in the nucleus and synapses (green) (**D**). RPE flatmounts stained with ZO-1 (green) show polygonal mononuclear cells in controls (G). *Slc9a8* mutant RPE cells are more irregular with multi-nucleated cells (H). Scale bars: 50 μm (**A**, **B**, **E**, **F**), 10 μm (**C**-**D**). Abbreviations as in Figure 3

Figure 5: Electroretinography of *Slc9a8*$^{tm1a(KOMP)Wtsi}$ mutant mice

A,D,G: ERGs of control (black traces) and *Slc9a8* mutant (grey traces) mice measuring rod responses in dark adapted mice (**A,D**) and cone responses in light-adapted mice (**G**). **B**: a-wave amplitude and implicit time of control and mutant mice in response to a dim flash. Amplitude shows a significant reduction in mutants but the implicit time is not different **C**: b-wave amplitude and implicit time of control and mutant mice in response to a dim flash. Amplitude shows a significant reduction in mutants and implicit time has a significant increase. **E**. In response to a bright stimulus, mutant mice have a reduced a-wave amplitude and longer implicit time. **F**. b-wave amplitude and implicit time in response to a bright stimulus shows a decrease in amplitude and increase in implicit time **H**. b-wave response of light adapted mice to a bright stimulus (cone pathway) shows mutant mice have a reduced amplitude and longer implicit time Means, SEM and statistics are in Supplementary Table 4. **I**. Dark-adapted, bright flash b-wave to a-wave ratio is significantly higher in mutant mice (3.070 ± 0.1097 (mean±SEM, n=7)) than in controls (1.925 ± 0.03967 (mean±SEM, n=8)) (Unpaired t test with Welch's correction $p< 0.0001$, $t=9.821$, $df=7.562$).

ns= P>0.05, * ≤0.05, ** ≤0.01, *** ≤0.001, **** ≤0.0001

Figure 6: Loss of *Slc9a8* in the RPE Alone Causes the Mutant Phenotype

The *Slc9a8*$^{tm1a(KOMP)Wtsi}$ allele was converted to the conditional *Slc9a8*$^{tm1c(KOMP)Wtsi}$ (*Slc9a8*^{con}) allele by crossing with a mouse expressing Flpe in the germ line. Fundus imaging shows a normal appearance of the retina of homozygous *Slc9a8*^{con} mice (**A**). Retinal histology of a homozygous *Slc9a8*^{con} eye, haematoxylin and eosin stained,

shows normal morphology(**C**). Fundus imaging of a retinas of 8 week old mice homozygous for *Slc9a8*^{con} and hemizygous for the RPE-specific *Tyr-Cre* transgene shows the same phenotype as a constitutive knockout (**B**). Haematoxylin and eosin stained section of a retina from the mouse in B, at 12 weeks, shows mutant retina produced by an RPE-specific knockout of *Slc9a8*. (**D**) We have analysed 4 mice which show the retinal phneotype from 2 separate litters. Fluorescence imaging of a retina from R26^{MTMG} mouse crossed with *Tyr-Cre* demonstrating activity of Cre only in the RPE (showing green fluorescent protein) and not in the other retinal layers (showing red, tomato, fluorescence) (**E**). Scale bars: 50μm (**A**, **C**) and 100μm (**D**) Abbreviations as in Figure 3

Figure 7: NHE8 localises to the Trans-Golgi Network and Recycling Endosomes

A. Localisation of HA tagged NHE8 protein in RPE1 cells, previously demonstrated to be found in the trans Golgi network (TGN) of HeLa cells[5]. **B**. mKate-tagged NHE8 shows a similar pattern of localisation in RPE1 cells. **C-E**. NHE8-mKate co-localises with the TGN marker, GFP-tagged GalT (arrows) and **F-H** with the recycling endosome (re)marker transferrin receptor (arrows) (**F**-**H**). Nuclei demarked with 'n'. All scale bars: 10 μm.

Figure 8: Loss of *Slc9a8* results in changes in recycling endosome morphology

Quantification of the mean volume of each recycling endosome in WT and *Slc9a8*$^{tm1a(KOMP)Wtsi}$ homozygous mutant mouse embryonic fibroblasts shows a statistically significant difference between WT and homozygous *Slc9a8*$^{tm1a(KOMP)Wtsi}$ (Hom). (Unpaired Student's t test, *P < 0.05)

References

1. White JK, Gerdin AK, Karp NA, et al. Genome-wide generation and systematic phenotyping of knockout mice reveals new roles for many genes. *Cell* 2013;154:452-464.
2. Donowitz M, Ming Tse C, Fuster D. SLC9/NHE gene family, a plasma membrane and organellar family of Na(+)/H(+) exchangers. *Molecular aspects of medicine* 2013;34:236-251.
3. Avila MY, Seidler RW, Stone RA, Civan MM. Inhibitors of NHE-1 Na+/H+ exchange reduce mouse intraocular pressure. *Investigative ophthalmology & visual science* 2002;43:1897-1902.
4. Brett CL, Tukaye DN, Mukherjee S, Rao R. The yeast endosomal Na+K+/H+ exchanger Nhx1 regulates cellular pH to control vesicle trafficking. *Molecular biology of the cell* 2005;16:1396-1405.
5. Lawrence SP, Bright NA, Luzio JP, Bowers K. The sodium/proton exchanger NHE8 regulates late endosomal morphology and function. *Molecular biology of the cell* 2010;21:3540-3551.
6. Cox GA, Lutz CM, Yang CL, et al. Sodium/hydrogen exchanger gene defect in slow-wave epilepsy mutant mice. *Cell* 1997;91:139-148.
7. Bell SM, Schreiner CM, Schultheis PJ, et al. Targeted disruption of the murine Nhe1 locus induces ataxia, growth retardation, and seizures. *The American journal of physiology* 1999;276:C788-795.
8. Ouyang Q, Lizarraga SB, Schmidt M, et al. Christianson syndrome protein NHE6 modulates TrkB endosomal signaling required for neuronal circuit development. *Neuron* 2013;80:97-112.
9. Schultheis PJ, Clarke LL, Meneton P, et al. Targeted disruption of the murine Na+/H+ exchanger isoform 2 gene causes reduced viability of gastric parietal cells and loss of net acid secretion. *The Journal of clinical investigation* 1998;101:1243-1253.
10. Schultheis PJ, Clarke LL, Meneton P, et al. Renal and intestinal absorptive defects in mice lacking the NHE3 Na+/H+ exchanger. *Nature genetics* 1998;19:282-285.
11. Gawenis LR, Greeb JM, Prasad V, et al. Impaired gastric acid secretion in mice with a targeted disruption of the NHE4 Na+/H+ exchanger. *The Journal of biological chemistry* 2005;280:12781-12789.
12. Goyal S, Vanden Heuvel G, Aronson PS. Renal expression of novel Na+/H+ exchanger isoform NHE8. *American journal of physiology Renal physiology* 2003;284:F467-473.
13. Xu H, Zhang B, Li J, Wang C, Chen H, Ghishan FK. Impaired mucin synthesis and bicarbonate secretion in the colon of NHE8 knockout mice. *American journal of physiology Gastrointestinal and liver physiology* 2012;303:G335-343.
14. Becker AM, Zhang J, Goyal S, et al. Ontogeny of NHE8 in the rat proximal tubule. *American journal of physiology Renal physiology* 2007;293:F255-261.
15. Xu H, Li J, Chen H, Wang C, Ghishan FK. NHE8 plays important roles in gastric mucosal protection. *American journal of physiology Gastrointestinal and liver physiology* 2013;304:G257-261.
16. Xu H, Zhao, Y., Li, J., Wang, M., Lian, F., Gao, M., Ghishan, F. K. Loss of NHE8 expression impairs ocular surface function in mice. *American journal of physiology Cell physiology* 2014;ajpcell.00296.02014.
17. Kleinjan DA, Seawright A, Mella S, et al. Long-range downstream enhancers are essential for Pax6 expression. *Developmental biology* 2006;299:563-581.

18. Delmas V, Martinozzi S, Bourgeois Y, Holzenberger M, Larue L. Cre-mediated recombination in the skin melanocyte lineage. *Genesis (New York, NY : 2000)* 2003;36:73-80.
19. Muzumdar MD, Tasic B, Miyamichi K, Li L, Luo L. A global double-fluorescent Cre reporter mouse. *Genesis (New York, NY : 2000)* 2007;45:593-605.
20. Wallace HA, Marques-Kranc F, Richardson M, et al. Manipulating the mouse genome to engineer precise functional syntenic replacements with human sequence. *Cell* 2007;128:197-209.
21. Schneider CA, Rasband WS, Eliceiri KW. NIH Image to ImageJ: 25 years of image analysis. *Nature methods* 2012;9:671-675.
22. Haddadin RI, Oh DJ, Kang MH, et al. Thrombospondin-1 (TSP1)-null and TSP2-null mice exhibit lower intraocular pressures. *Investigative ophthalmology & visual science* 2012;53:6708-6717.
23. Skarnes WC, Rosen B, West AP, et al. A conditional knockout resource for the genome-wide study of mouse gene function. *Nature* 2011;474:337-342.
24. Aleman TS, Cideciyan AV, Aguirre GK, et al. Human CRB1-associated retinal degeneration: comparison with the rd8 Crb1-mutant mouse model. *Investigative ophthalmology & visual science* 2011;52:6898-6910.
25. Mattapallil MJ, Wawrousek EF, Chan CC, et al. The Rd8 mutation of the Crb1 gene is present in vendor lines of C57BL/6N mice and embryonic stem cells, and confounds ocular induced mutant phenotypes. *Investigative ophthalmology & visual science* 2012;53:2921-2927.
26. Longbottom R, Fruttiger M, Douglas RH, Martinez-Barbera JP, Greenwood J, Moss SE. Genetic ablation of retinal pigment epithelial cells reveals the adaptive response of the epithelium and impact on photoreceptors. *Proceedings of the National Academy of Sciences of the United States of America* 2009;106:18728-18733.
27. Xu H, Chen H, Li J, Zhao Y, Ghishan FK. Disruption of NHE8 Expression Impairs Leydig cell function in the testes. *American journal of physiology Cell physiology* 2014;ajpcell.00289.02014.
28. Liu C, Xu H, Zhang B, et al. NHE8 plays an important role in mucosal protection via its effect on bacterial adhesion. *American journal of physiology Cell physiology* 2013;305:C121-128.
29. Gibbs D, Kitamoto J, Williams DS. Abnormal phagocytosis by retinal pigmented epithelium that lacks myosin VIIa, the Usher syndrome 1B protein. *Proceedings of the National Academy of Sciences of the United States of America* 2003;100:6481-6486.
30. Petrukhin K, Koisti MJ, Bakall B, et al. Identification of the gene responsible for Best macular dystrophy. *Nature genetics* 1998;19:241-247.
31. Marquardt A, Stohr H, Passmore LA, Kramer F, Rivera A, Weber BH. Mutations in a novel gene, VMD2, encoding a protein of unknown properties cause juvenile-onset vitelliform macular dystrophy (Best's disease). *Human molecular genetics* 1998;7:1517-1525.
32. Kramer F, White K, Pauleikhoff D, et al. Mutations in the VMD2 gene are associated with juvenile-onset vitelliform macular dystrophy (Best disease) and adult vitelliform macular dystrophy but not age-related macular degeneration. *European journal of human genetics : EJHG* 2000;8:286-292.
33. Yu K, Qu Z, Cui Y, Hartzell HC. Chloride channel activity of bestrophin mutants associated with mild or late-onset macular degeneration. *Investigative ophthalmology & visual science* 2007;48:4694-4705.
34. Kao L, Kurtz LM, Shao X, et al. Severe neurologic impairment in mice with targeted disruption of the electrogenic sodium bicarbonate cotransporter NBCe2 (Slc4a5 gene). *The Journal of biological chemistry* 2011;286:32563-32574.

A

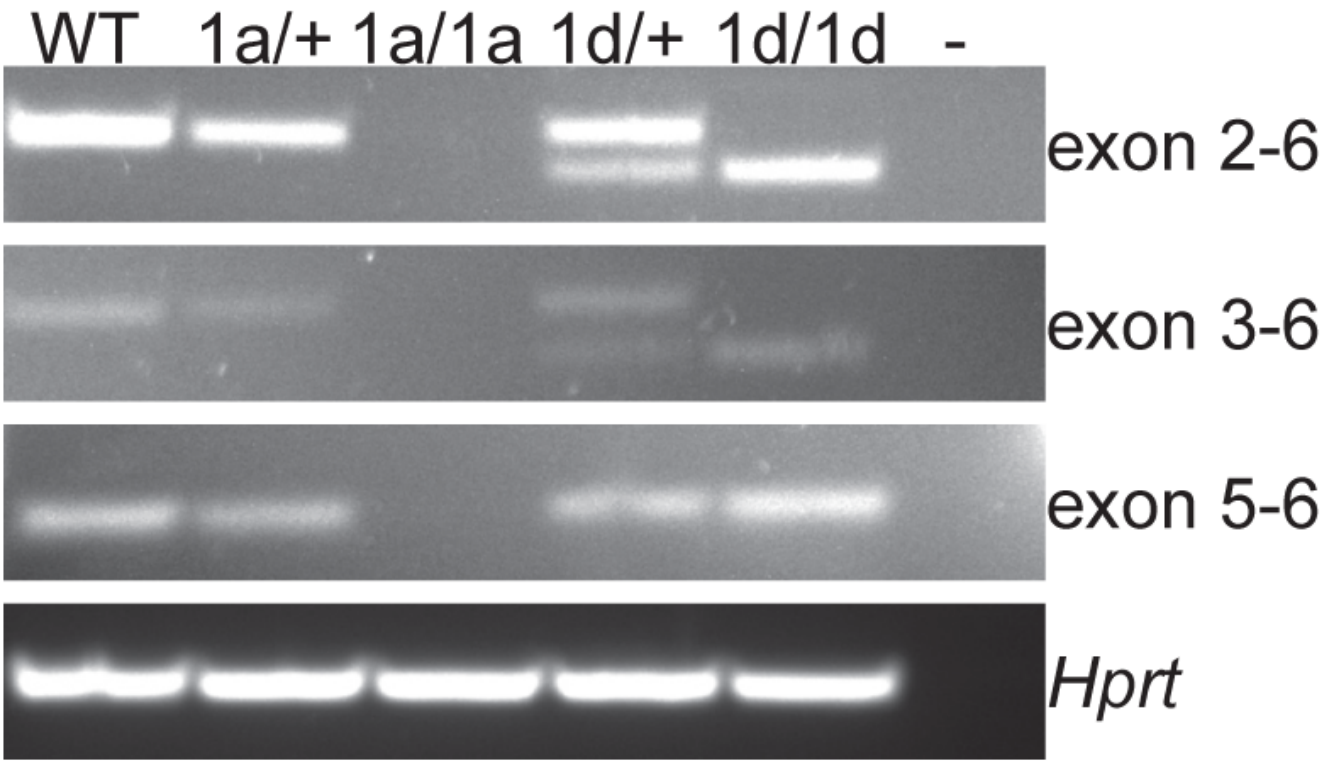

B

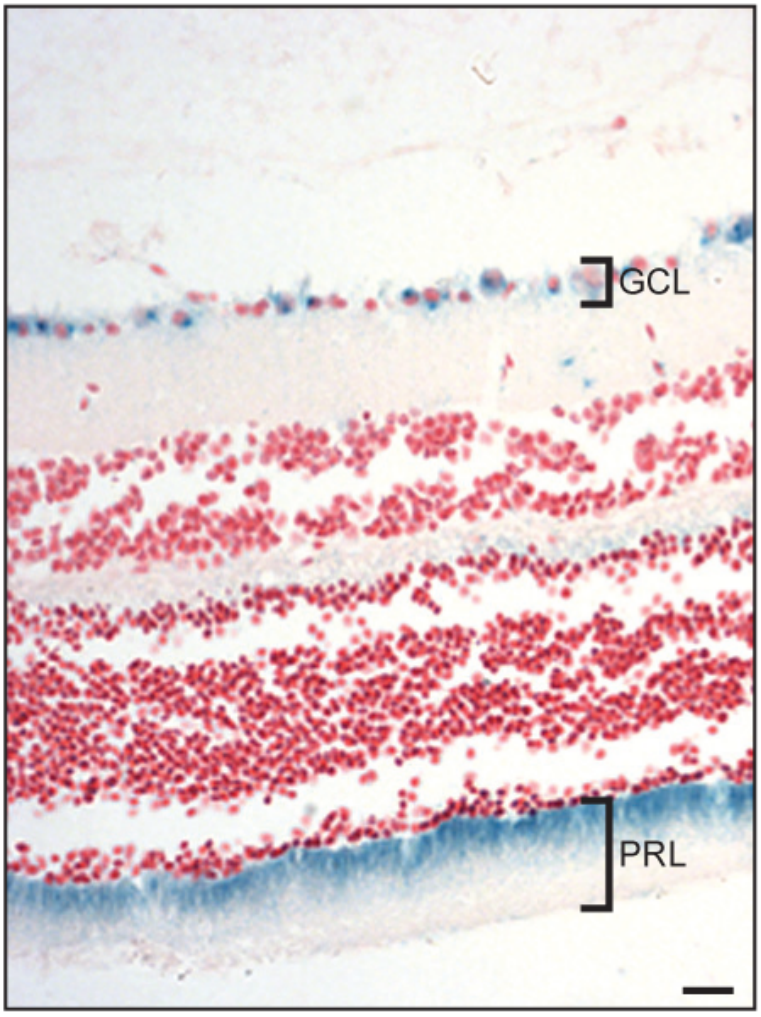

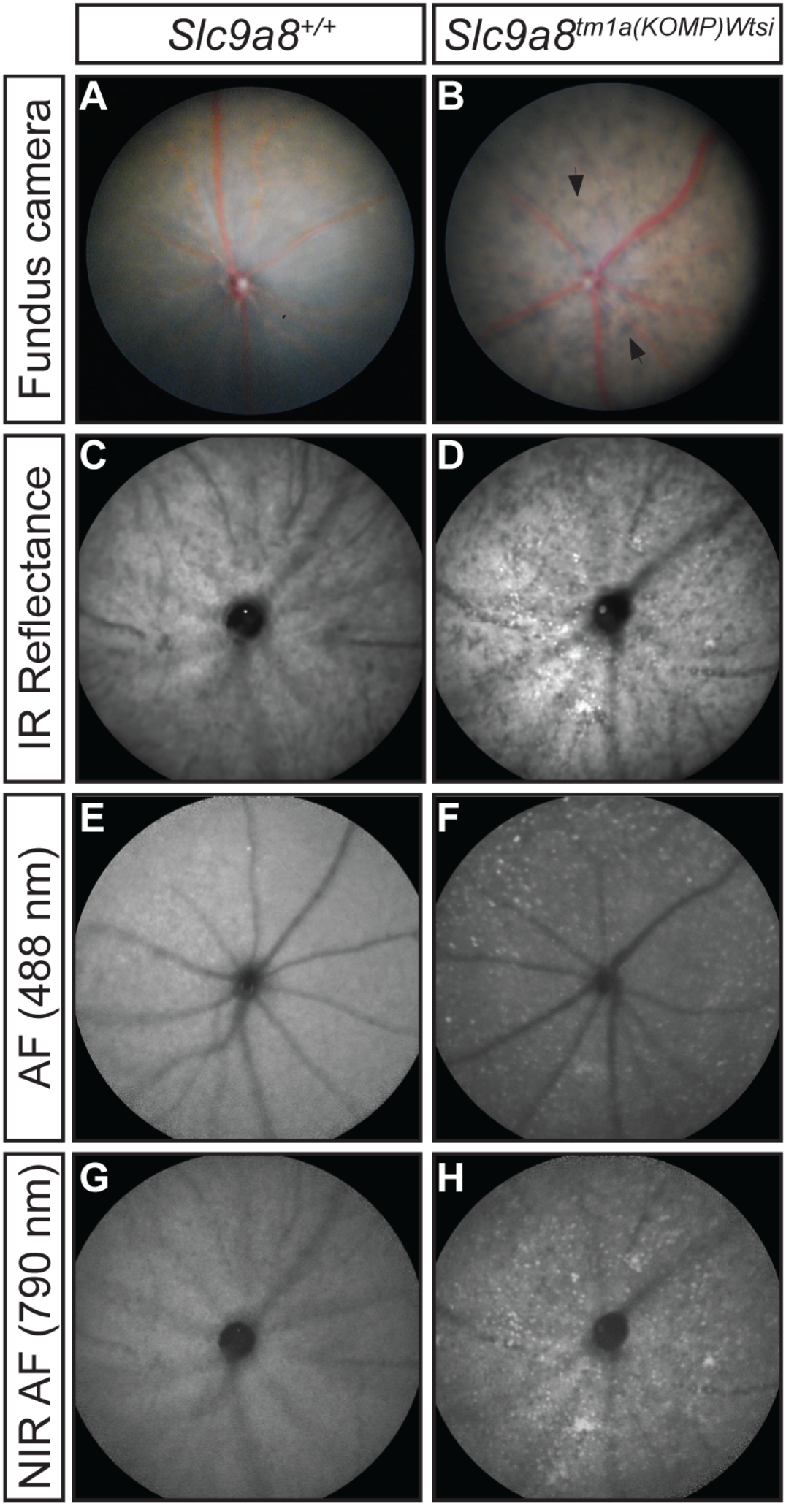
Slc9a8+/+
Slc9a8tm1a(KOMP)Wtsi
Fundus camera
IR Reflectance
AF (488 nm)
NIR AF (790 nm)
A
B
C
D
E
F
G
H

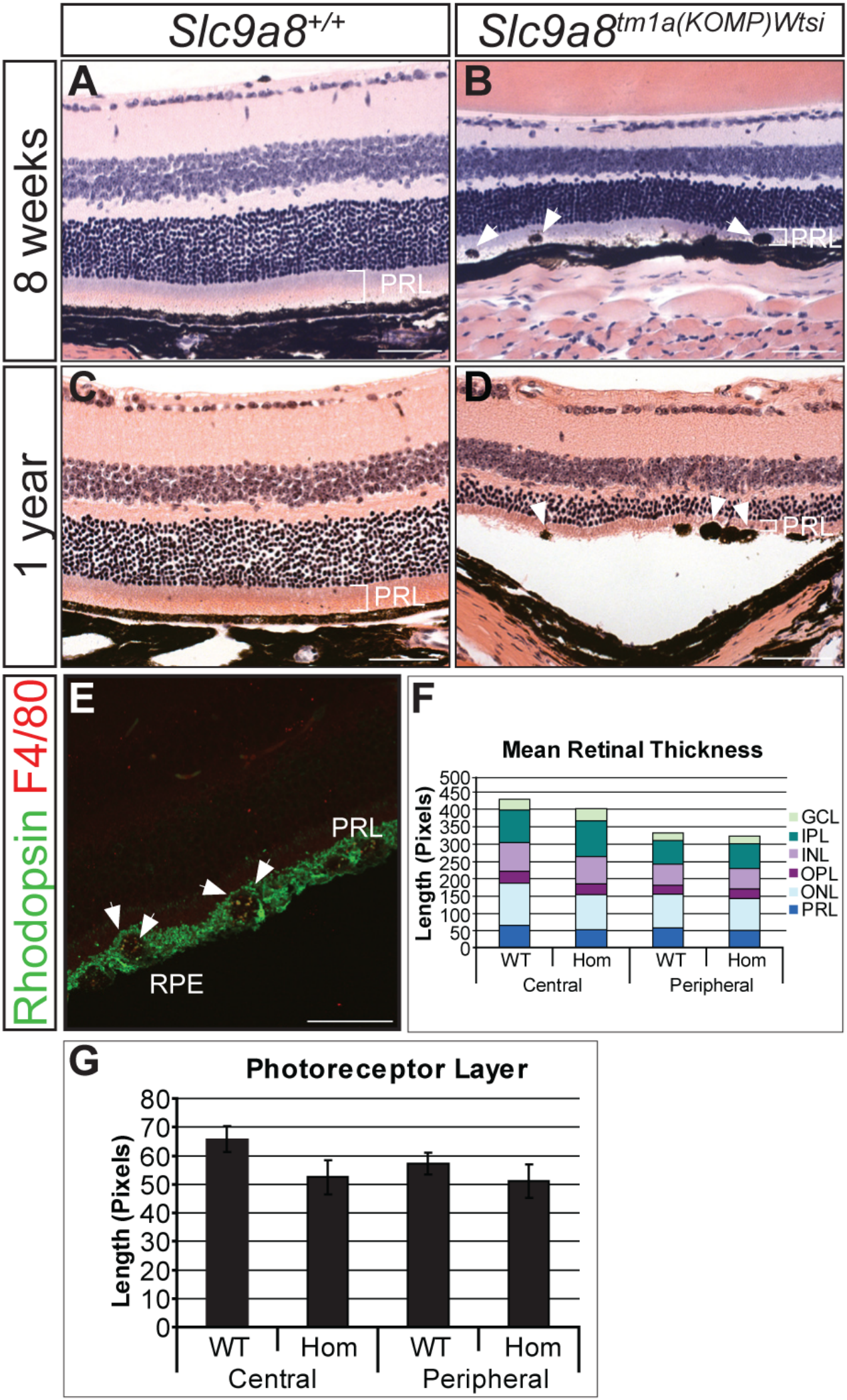
Slc9a8+/+
Slc9a8tm1a(KOMP)Wtsi
8 weeks
1 year
A
B
C
D
PRL
Rhodopsin F4/80
E
RPE
F
Mean Retinal Thickness
Length (Pixels)
500
450
400
350
300
250
200
150
100
50
0
GCL
IPL
INL
OPL
ONL
PRL
WT
Hom
Central
Peripheral
G
Photoreceptor Layer
80
70
60
50
40
30
20
10
0

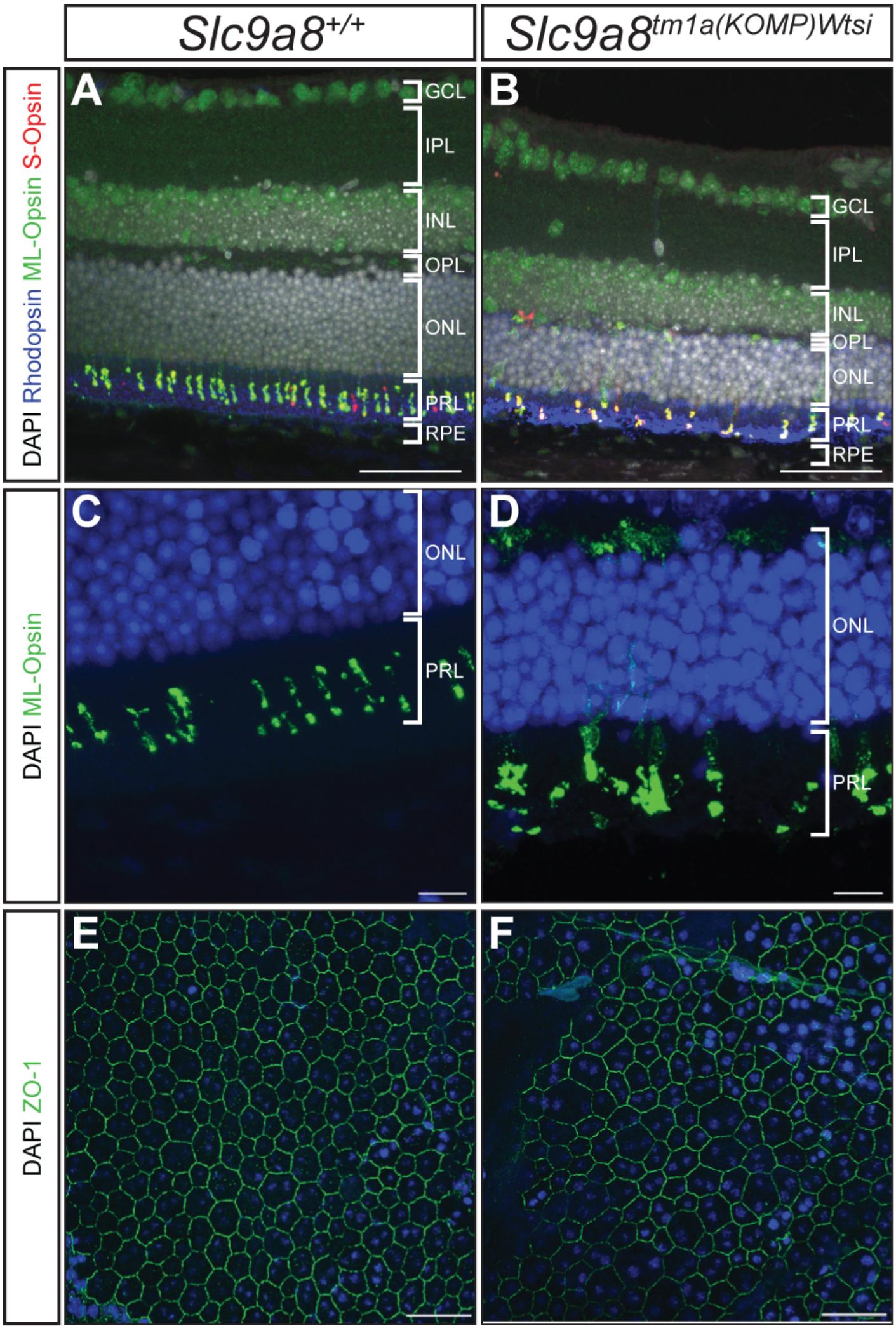
Slc9a8+/+
Slc9a8tm1a(KOMP)Wtsi
DAPI Rhodopsin ML-Opsin S-Opsin
A
B
GCL
IPL
INL
OPL
ONL
PRL
RPE
DAPI ML-Opsin
C
D
ONL
PRL
DAPI ZO-1
E
F

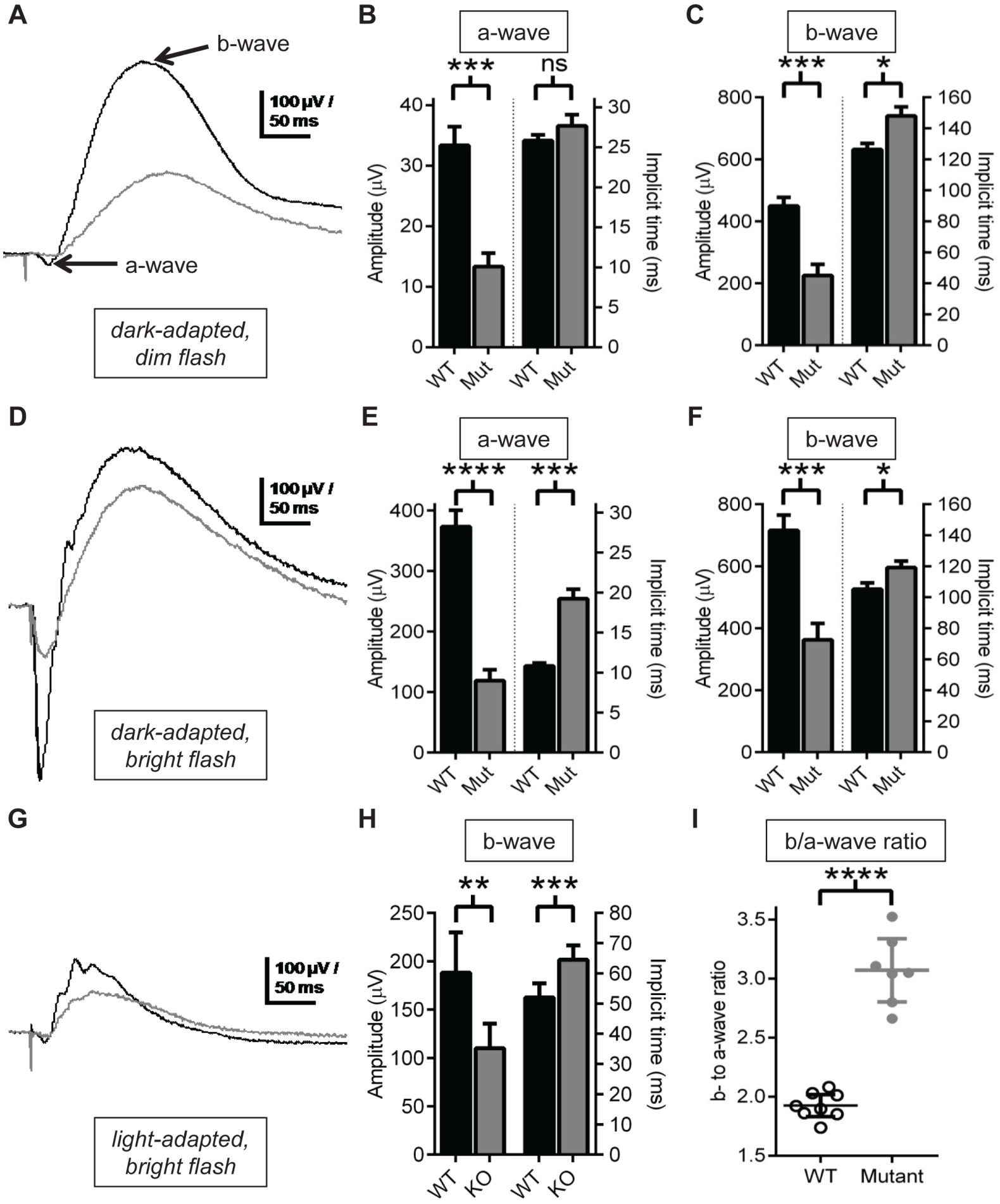
A
b-wave
a-wave
100 µV /
50 ms
dark-adapted,
dim flash
B
a-wave
***
ns
Amplitude (µV)
Implicit time (ms)
WT
Mut
C
b-wave
***
*
D
dark-adapted,
bright flash
E
a-wave
****
***
F
b-wave
***
*
G
light-adapted,
bright flash
H
b-wave
**
***
KO
I
b/a-wave ratio
****
b- to a-wave ratio
Mutant

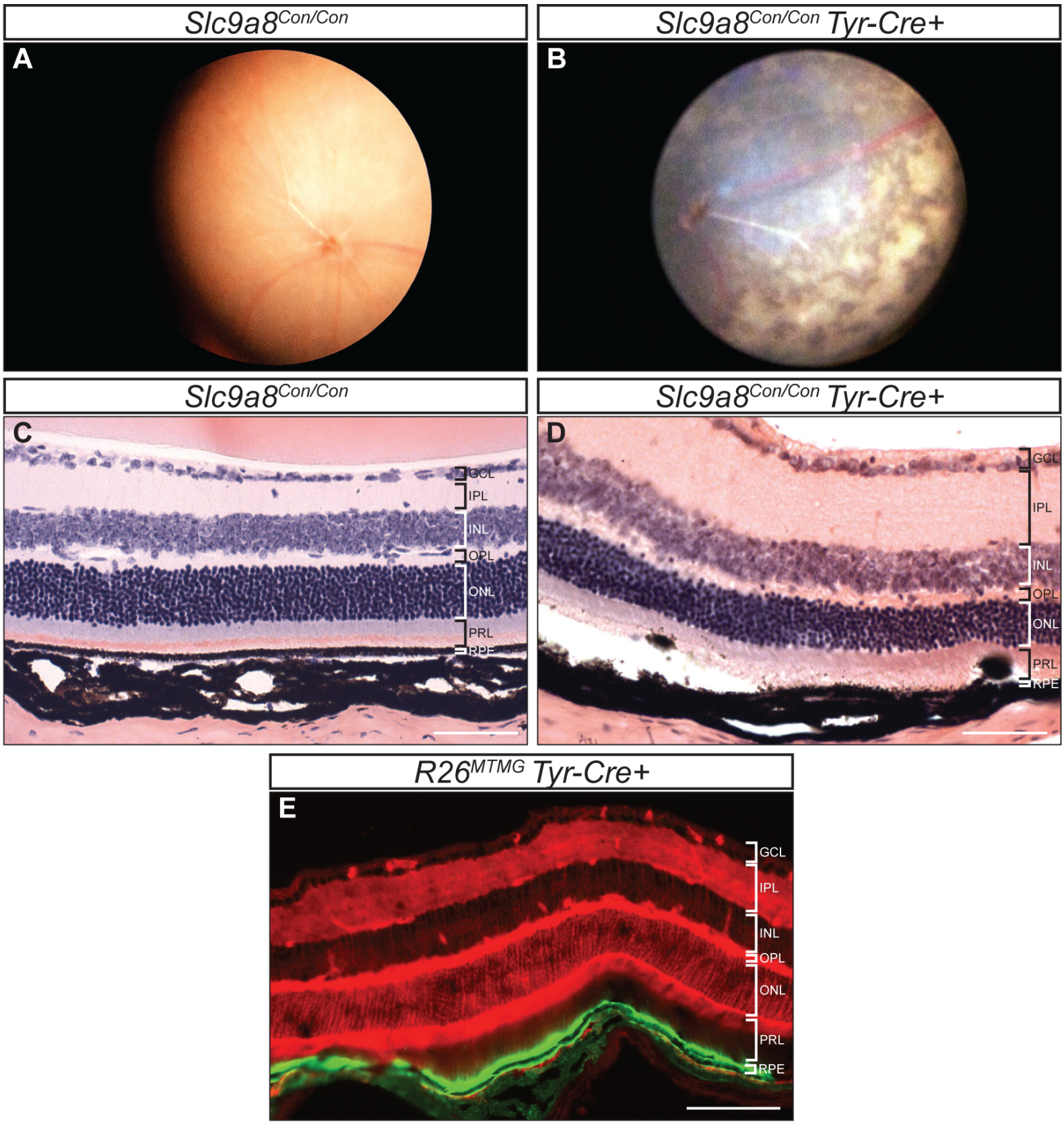
Slc9a8Con/Con
A
Slc9a8Con/Con Tyr-Cre+
B
Slc9a8Con/Con
C
GCL
IPL
INL
OPL
ONL
PRL
RPE
Slc9a8Con/Con Tyr-Cre+
D
GCL
IPL
INL
OPL
ONL
PRL
RPE
R26MTMG Tyr-Cre+
E
GCL
IPL
INL
OPL
ONL
PRL
RPE

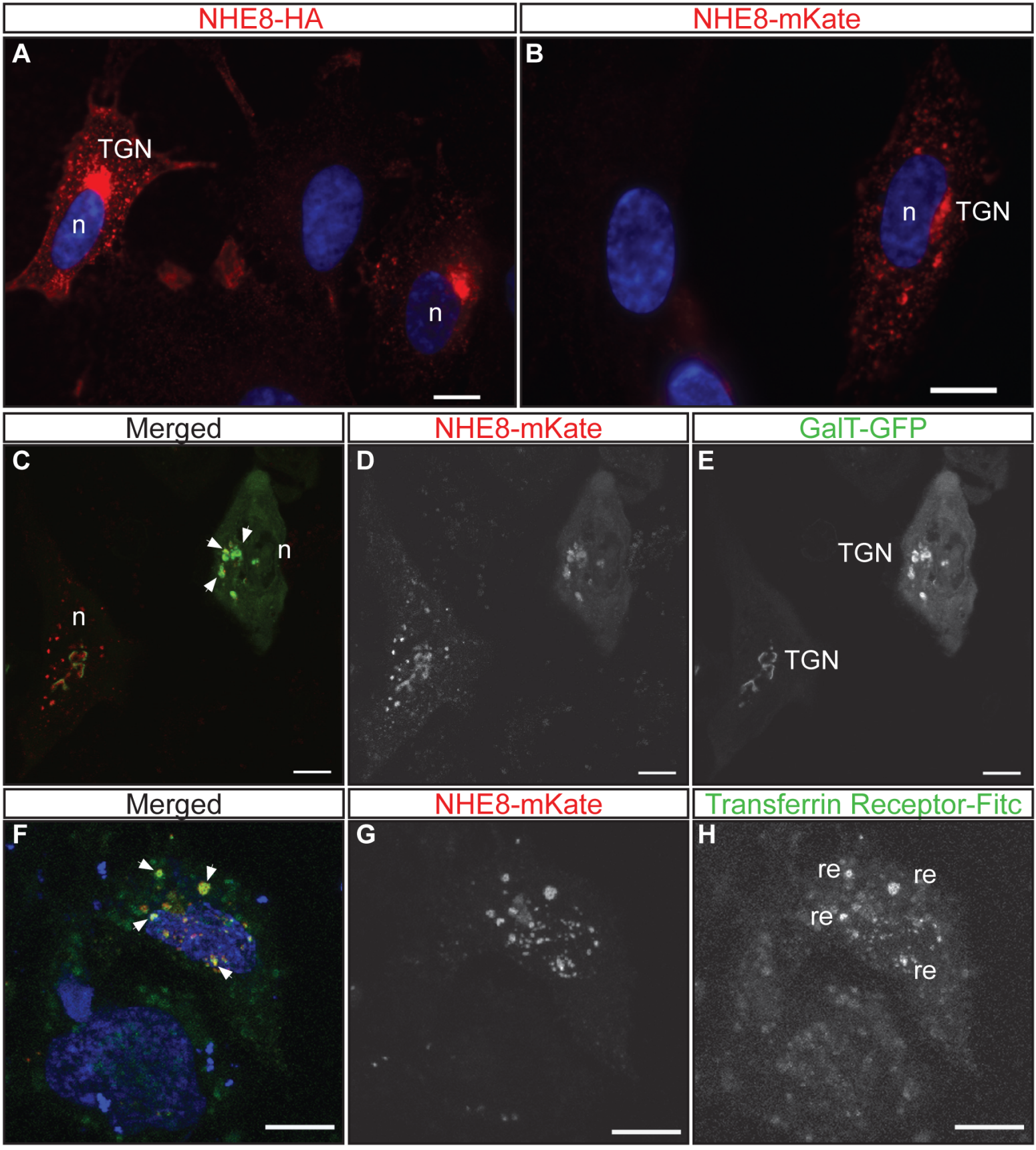
NHE8-HA
NHE8-mKate
A
TGN
n
n
B
n
TGN
Merged
NHE8-mKate
GalT-GFP
C
n
n
D
E
TGN
TGN
Merged
NHE8-mKate
Transferrin Receptor-Fitc
F
G
H
re
re
re
re

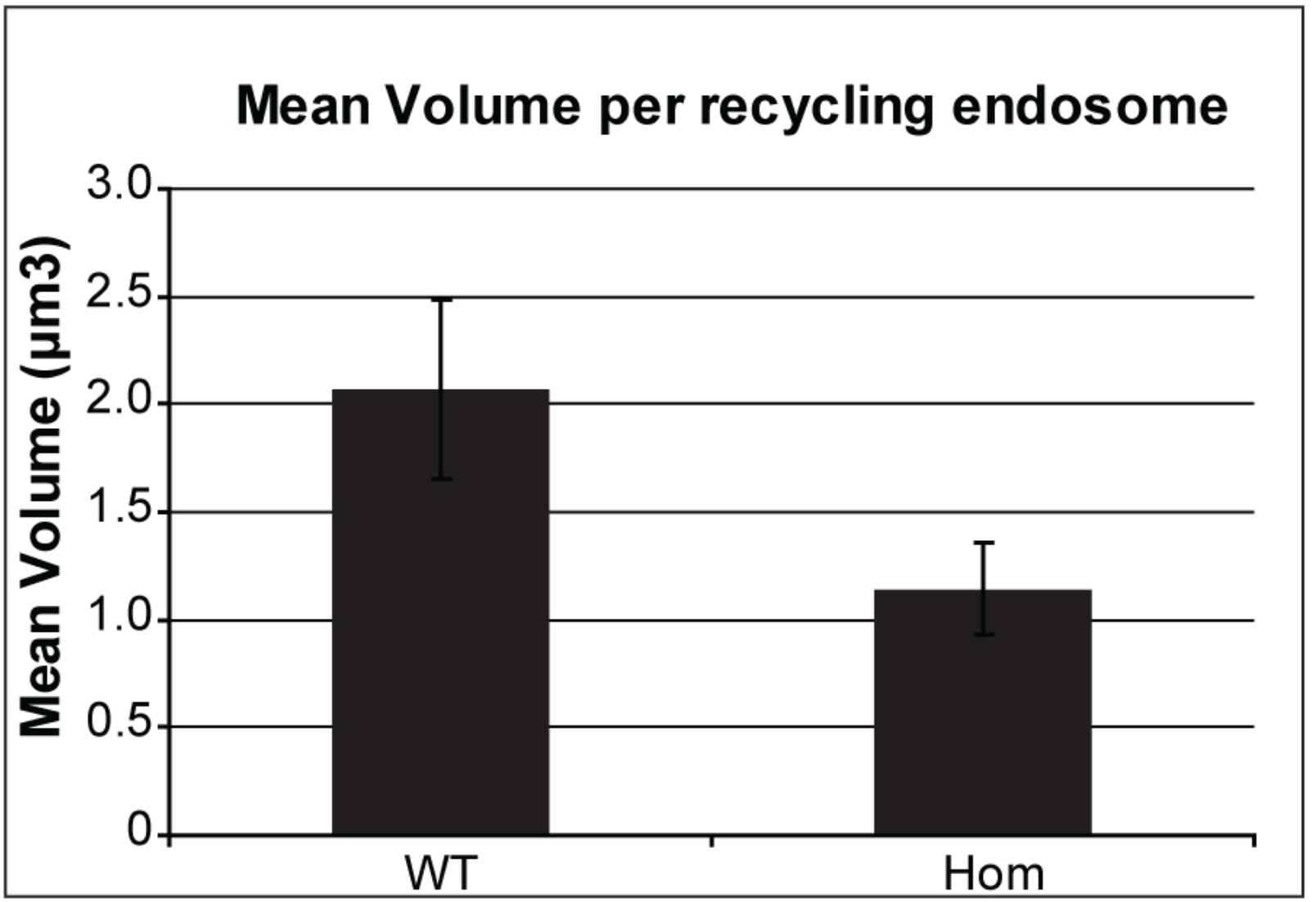
Mean Volume per recycling endosome
Mean Volume (µm3)
3.0
2.5
2.0
1.5
1.0
0.5
0
WT
Hom